Int. J. Electrochem. Sci., 11 **(2016)** 4909 – 4921, doi: 10.20964/2016.06.76

International Journal of ELECTROCHEMICAL SCIENCE
www.electrochemsci.org

Electrochemical Formation and Selenization of Ternary CuZnSn Alloys for Growing $Cu_2ZnSnSe_4$ Photoactive Thin Films

Mohamed Benaicha[*], *Meriem Hamla, Sabrine Derbal*

Energetic and Solid-State Electrochemistry Laboratory, Faculty of Technology, Ferhat Abbas-Setif1 University, Setif, 19000, Algeria.
[*]E-mail: mdbenaicha@yahoo.fr

Received: 19 March 2016 / *Accepted:* 25 April 2016 / *Published:* 4 May 2016

A two-step electrochemical route for the synthesis of $Cu_2ZnSnSe_4$ (CZTSe) photoactive thin films is reported in this work. A ternary Cu-Zn-Sn (CZT) alloy was electrochemically deposited onto Indium doped Tin Oxide (ITO) substrates from citrate electrolyte followed by a thin layer of Se on the top. The CZT + Se deposits were annealed under vacuum and characterized by means of field emission scanning electron microscopy (FESEM), energy dispersive spectrometry (EDS), X-ray diffraction (XRD), Raman spectroscopy and UV-VIS spectroscopy respectively. The XRD measurements indicated that when annealed under vacuum at 350 °C, the manufactured CZT+ Se precursors contained the main diffraction peaks of CZTSe in addition to secondary phases such as Cu_6Sn_5 and Cu_5Zn_8 binaries. With increasing temperature up to 550 °C, the CZTSe deposits presented stannite structure with a band gap of 1.12 eV and contained traces of Cu_2SnSe_3 phase.

Keywords: $Cu_2ZnSnSe_4$; Solar cells; thin films; Selenization; Electrodeposition

1. INTRODUCTION

$Cu_2ZnSnSe_4$ (CZTSe) compound has attracted much attention recently as one of the most promising candidates to replace conventional absorber materials such as CdTe and $CuIn_{1-x}Ga_xSe_2$ (CIGSe). Due to its many advantages including low toxicity, abundance in the Earth's crust and low cost of its constituents (Copper, Zinc and Tin prices are low at approximately 10 $/Kg, contrary to Indium whose price is almost 1,000 $/Kg), CZTSe is thought to be more suitable for mass production. On the other hand, in addition to their long-term stability, CZTSe and its derivates CZTSSe have valuable properties such as a tunable direct band gap (1.0 – 1.5 eV) and a high absorption coefficient

in the visible range (~ $10^4 – 10^5$ cm^{-1}) [1-2] so that the material utilization can be reduced, with 1–2 μm layer thickness generally being enough to absorb most of the incident solar radiation. Up to now, the highest conversion efficiency of ~9.15% was obtained for devices based on co-evaporated CZTSe thin films [3-4]. To fabricate CZTSe films of photovoltaic (PV) grade, various approaches have been reported, including thermal co-evaporation [3-6], magnetron sputtering [7], pulsed laser deposition [8], spray pyrolysis [9] and electrodeposition [10-13].

Compared to the costly vacuum technologies, the electrochemical method has various advantages, such as its simplicity, low processing cost, no need for very pure stating materials (based on automatic purification of the deposited materials during plating), minimum waste generation (the solution can be recycled), no need for vacuum systems or use of toxic gases. Some attempts to deposit $Cu_2ZnSnSe_4$ in a single step from aqueous electrolytes were reported [14] but both the as-deposited and annealed films had structural failures. The broad peaks seen in the Raman spectra suggested insufficient crystallinity and presence of large amounts of bulk defects.

The electrodeposition of the quaternary Cu-Zn-Sn-Se system is rather difficult since its constituents are significantly disparate with respect to their equilibrium potentials and due to the instability of the electrolyte as a result of strong interactions between Se and Sn salts. Therefore, CuZnSn alloys and Se must be deposited separately. The conditions for electroplating CuZnSn thin films are related to the electrochemical deposition reactions for each element following Nernst formula:

$$M^{z+} + ze^- \leftrightarrows M$$

$$E_M = E_0 + \frac{RT}{zF}\ln\left(\frac{a_{M^{z+}}}{a_M}\right)$$

Where E_M and E_0 are the equilibrium and standard electrode potentials with respect to the reference electrode, $a_{M(z+)}$ and a_M the activities of the cations in the solution and that of the atoms in the deposit. For selenium deposition, the process is influenced by the acidity (pH) of the solution:

$$H_2SeO_3 + 4H^+ + 4e^- \leftrightarrows Se(s) + 3H_2O$$

$$E_{Se^{4+}/Se} = +0.778 + 0.0148\ log\ a_{HSeO_2^+} - 0.0739\ pH$$

The value of 0.778 is the standard electrode potential of Se. The equilibrium potential of the reaction could be reduced mainly by increasing pH which in turn leads to precipitation of zinc ions in the form of hydroxide. This confirms that CuZnSn and Se layers have to be deposited from separate baths. Therefore, in order to co-deposit Cu, Zn and Sn, it is possible to adjust the composition of the solution to bring closer the equilibrium potentials of the three elements. However, the use of simple electrolytic solutions generally leads to the formation of powdery or non-adherent layers which are unusable for most practical applications. In addition, in such simple baths, another major problem regarding the electrodeposition of Cu -Zn-Sn alloys appears: The simultaneous presence of Sn(II) and Cu(II) species facilitates the reduction of Cu (II) to metallic copper by Sn(II) ions and causes the instability of the solution.

Choosing a suitable complexing agent may shift the equilibrium potentials and stabilize the electrolytic baths by changing the dominant tin(II) and copper(II)species. On the other hand, due to the narrow compositional range for stoichiometric kesterite compounds [15], subsequent selenization and/or sulfurisation of the electrodeposited films are needed. Successful experiments of synthesis of

stoichiometric $Cu_2ZnSnSe_4$ (CZTSe) have been carried out by Ganchev *et al*. [10-11] via selenization of stacked metallic CuZn/CuSn precursors sequentially electrodeposited from an aqueous pyrophosphate –type formulation and Chen *et al*. [16] by vapor selenization of ternary CuZnSn alloy deposited from a citrate electrolyte. However, the conventionally used technique employing H_2Se gas or Se vapor is not a safe method for large –scale production. More recently, Delbos et al.[17] reported a successful synthesis technique of CZTSe using chemical deposition of selenium onto electrodeposited or sputtered CuZnSn substrates, followed by an annealing step.

In this work, we report an electrochemical route for the formation of CZTSe thin films from citrate plating bath, via a two-stage process. Firstly, ternary Cu-Zn-Sn metallic precursors were co-electroplated onto ITO glass substrates followed by deposition of a thin layer of selenium on the top. The as-prepared precursors were then annealed under vacuum for half an hour at a range of temperatures between 350 and 550 °C. The structural, compositional, morphological and optical properties of the CZTSe films were investigated using X-ray diffraction (XRD), energy dispersive spectrometry (EDS), Raman spectroscopy, field emission scanning electron microscopy (FESEM) and UV-Vis spectroscopy respectively.

2. EXPERIMENTAL DETAILS

The electrochemical experiments were performed in a conventional three electrodes electrochemical cell containing 75 ml solution, with a Voltalab potentiostat-galvanostat (model PGZ 301) to run cyclic voltammetry or to deposit the thin films under potentiostatic regime. All the plating solutions were prepared by dissolving chemicals (Sigma-Aldrich, USA) of highest purity (99.99%) without need for further purification, in doubly distilled water to give 10 mM $CuCl_2$, 15 mM $SnCl_2$, 25mM $ZnCl_2$ and 50 mM SeO_2 **.** The pH of the bath was maintained at 4.2 to avoid precipitation of zinc hydroxide**.** The concentration on tri-sodium citrate ($C_6H_5O_7Na_3$) used as a complexing agent was as high as 400 mM to form strong complexes and to ovoid precipitation of insoluble salts, mainly copper powder [18]. Citrate-based aqueous plating electrolytes are environmentally friendly and the citrate ions form electroactive and stable complexes with Cu(II), Sn(II), Zn(II) and Se(IV) active species. However, selenium salt was not added to the CuSnZn (CZT) plating bath since it oxidizes Sn(II) to Sn(IV) even though in the presence of anti-oxidant agents. Consequently, selenium was deposited separately from an acidic electrolyte containing the selenium salt and tri-sodium citrate. For the electrochemical investigations, a platinum mesh with 0.5 cm^2 exposed area was used as working electrode. Sheets sized 1x 2 cm^2 of commercially available indium-doped tin oxide (ITO)-coated glass with resistance of 12 Ω/cm^2 and transmittance of 75-85 % in the visible range (Solems, France) were used as substrates for the characterization of CZT precursors and the final synthesis of CZTSe thin films respectively. The cyclic voltammograms (CVs) were recorded at a scan rate of 50 $mV.s^{-1}$, scanned first towards cathodic direction. The cathodic deposition of the films was carried out in an unstirred bath at room temperature. Prior to the deposition, the substrates were ultrasonically cleaned with acetone, activated for few seconds in hot hydrochloric acid solution and finally rinsed with ultra pure water. In all cases, a platinum foil of high active surface area was used as the auxiliary electrode

and a saturated calomel electrode (SCE) as the reference to which all potentials in this paper are referred. After the precursors (metallic CuZnSn and Se thin layers) were deposited, they were put into a quartz tube connected to a high speed vacuum pump (Adixen-Pfeiffer, Germany) allowing up to 10^{-7} mbar vacuum. The quartz tube was then introduced into a horizontal tube furnace (Thermolyne-Model 21100) with automatic temperature control accurate. After annealing, the specimens were cooled down naturally.

The structural quality of the samples was examined using X-ray diffraction (Philips X'Pert Pro Multipurpose X-ray diffractometer) with a Cu K_α radiation source ($\lambda_{K\alpha}$ =1.5418 Å). Room temperature (RT) micro-Raman scattering measurements were performed in the range of 100-1100 cm^{-1} with a confocal Raman spectrometer (Renishaw inVia micro-Raman system, United Kingdom) with integral plasma filter. Light source was a red HeNe Laser emitting at 632.8 nm in a single mode (TEM00, vertically polarized) - 17 mW output in the visible and providing a spectral resolution of 0.5 cm^{-1}.

The optical properties were analyzed by UV–Vis spectrophotometer (Shimadzu 1800) with UV-Probe software for the curves analysis. The optical absorption spectra were recorded at room temperature from 200 to 1100 nm. The thin films morphology and composition were investigated by a field-emission scanning electron microscope (FESEM, JEOL JSM-7100F) with an accelerating voltage of 20 kV and acquisition time of 90 s, and equipped with a high resolution silicon drift detector (SDD) for X-ray Energy Dispersive Spectroscope (EDS) microanalysis.

3. RESULTS AND DISCUSSION

3.1. Electrochemical analysis

In order to determine the thermodynamic characteristics of Cu, Zn and Sn in co-existence in citrate-based solution, cyclic voltammetry was used. The measurements were performed after the open circuit voltage (E_{oc}) of the electrochemical cell was stabilized (usually 15 min).

The voltammogram for an electrolyte containing copper (II), tin (II) and zinc (II) ions in the presence of tri-sodium citrate is presented in [Fg.1 (a)]. Due to the reduction over-potential appearing in solutions containing such a complexing agent, the real potential range for the electrodeposition of Cu, Sn and Zn are moved towards lower potentials. In all cases, a slight cathodic wave at the beginning of the scan up to -0.2 V is observed, corresponding most probably to the reduction of dissolved oxygen as the solution used was not de-aerated. The reduction of Cu^{2+}/Cu onto platinum starts first at approximately -0.24 V versus SCE and reaches its maximum at ~ -0.37 V versus SCE. The behavior of Sn^{2+}/Sn couple is similar to that for Cu^{2+}/Cu system, displaying a cathodic wave between -0.75 and -0.95 V followed by a reduction peak of Zn(II) ions ($Zn^{2+} + 2e^- \rightarrow Zn$) at around -1.3 V versus CSE. On the reverse scan, the voltammogram displays a crossover and an anodic signal attributable to the re-oxidation of Zn ($Zn \rightarrow Zn^{2+} + 2e^-$, peak A_1) at -1.1 V, two anodic peaks around -0.67 and – 0.49 mV/CSE related to the oxidation reactions of Sn ($Sn \rightarrow Sn^{2+} + 2e^-$, standard reduction potential ~ - 0.138 V/SHE, peak A_2) and Sn^{2+} ($Sn^{2+} \rightarrow Sn^{4+} + 2e^-$, standard reduction potential ~ + 0.151 V/SHE, peak A_3) respectively. At more positive potentials, two anodic

stripping peaks are observed in the (-0.2 - +0.35 V) region, corresponding to the re-oxidation of the previously deposited copper layer: ($Cu \rightarrow Cu^{2+} + 2e^-$, standard reduction potential ~ + 0.34 V/SHE, peak A_4 and $Cu \rightarrow Cu^{+} + e^-$, standard reduction potential ~ + 0.51 V/SHE, peak A_5). The presence of the crossover indicates the nuclei formation on the substrate [19]. The same shape of voltammograms was found for the ITO-coated glass substrates (not reported here) with a deviation of ~80 mV in the cathodic direction. In addition, the increase in the current density at potentials more negative than ~ -1.4 V can be attributed to the hydrogen evolution reaction (HER) occurring in parallel to CuZnSn deposition.

This part of study was useful to determine the adequate potential/current range for deposition of CuSnZn alloys. Thin films with a thickness of about 1 µm were grown under potentiostatic regime onto Platinum sheets in the range of -0.8 to -1.3 V versus CSE and analysed by EDS. The most suitable potential range for a nearly stoechiometric Cu_2ZnSn film was estimated to be in the (~ -1.05 to -1.10 V versus CSE) region. This result is in a good agreement with the reported one by Liu *et al*. [34]. The elements ratios $\frac{Cu}{Zn+Sn}$ in CZT layers are 1.12 and 0.97 for deposition potential of -1.05 and -1.1 V/CSE respectively, while their molar concentration ratio in the plating solution is relatively low (0.25).

To prepare CZTSe, the electrodeposited CZT films were used as substrates for selenium deposition. For the voltammetric study, Pt electrode was used instead of CZT to avoid interferences between Cu, Zn, Sn and Se deposit signals during the anodic scan. In both cases, the cathodic part of the curve has the same shape with a shift of about 60 mV in negative side for CZT substrates. Fg.1 (b) shows a typical cyclic voltammogram for Se electrodeposition on Pt electrode from a solution containg SeO_2 and tri-sodium citrate. The potential was swept between 1.2 and -1.5 V.vs CSE, starting from 0.3V (OCP) and initially conducted in the negative direction. The curve displays three well defined cathodic waves (labeled C1, C2 and C3) and one anodic wave (A) in addition to a crossover during the cathodic to anodic reverse scan. In combination with other studies [20-22], these voltammetric peaks can be assigned as follows: The initial cathodic wave (C1) in the potential range from +0.2V to -0.35V is usually associated with Se under potential deposition (UPD) process [23]. The second cathodic weak peak C2 at a potential of -0.75V corresponds to bulk selenium deposition:

$$H_2SeO_3 + 4H^+ + 4e^- \leftrightarrows Se + 3H_2O \qquad E^0 = 0.5V\ vs.CSE$$

The third reduction peak (C3) appearing at more negative potentials (about -1.0 V vs. CSE) and not associated to any anodic response, corresponds to the formation of the gaseous H_2Se species via a direct reduction of Se^{4+} to Se^{2-} according to the following reaction:

$$H_2SeO_3 + 6H^+ + 6e^- \rightarrow H_2Se + 3H_2O \qquad E^0 = 0.12V\ vs.CSE$$

At potentials more negative than -1.0 V, the current increases rapidly due to the hydrogen evolution reaction (HER). The presence of the nucleation loop after the reversal of the scan is diagnostic for the formation of selenium nuclei on Pt substrate. Finally, the anodic peak (A) at 0.7 V can be assigned to the oxidation of Se deposit to Se^{4+}. Based on these results, the suitable potential for the deposition of selenium on CZT substrates was chosen to be around -0.8 V vs. CSE.

3.2. Structural investigation

After selenium deposition on the top of the CuZnSn precursors, the samples were annealed under vacuum in a conventional annealing furnace, kept at a chosen temperature for 30 min, and then cooled down naturally to room temperature. The representative XRD patterns of annealed CuSnZn+Se films deposited ITO/glass substrates are shown in (Fig. 2). For low temperature annealing (350 °C), the main reflections at 28.54°, 44.56°, 54.98°, 65.18° and 72.69° attributable to stannite $Cu_2ZnSnSe_4$ compound [10,12,24] as well as signals corresponding to traces of copper binaries with Sn (η-Cu_6Sn_5, JCPDS# 03-065-2303) and Zn (γ-Cu_5Zn_8, JCPDS# 01-071-0397) were found in the XRD analysis. In addition, there are reflections of ITO substrate [25, 26] at angles 2Θ ~ 30.50°, 35.90°, 49.38° and 63.25°.

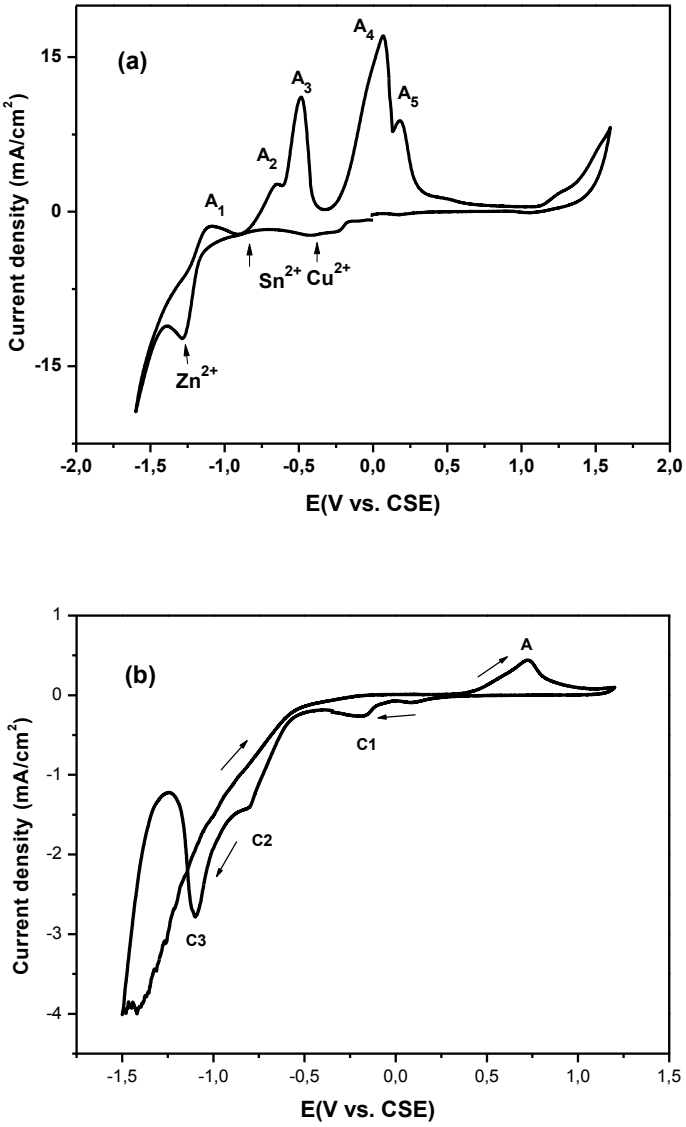

Figure 1. CVs (vs. CSE) recorded at room temperature with a sweep rate of 50 $mV.s^{-1}$ of solution at pH 4.2 containing 0.4 M $C_6H_5O_7Na_3$ (tri-sodium citrate) and: (a) 15 mM $CuCl_2$ + 50 mM $SnCl_2$ + 25 mM $ZnCl_2$, (b) 50 mM SeO_2

Annealing at 450 °C leads to significant changes in the XRD patterns. Further annealing up to 550 °C accentuates the intensity of the reflection lines of CZTSe and consequently improves the crystallinity of the electrodeposited layers. The grain sizes of the deposits were determined from X-ray patterns using the Scherrer's formula [27]:

$$d = \frac{0.9\lambda}{\beta cos\theta}$$

Where λ, θ and β are the wavelength of $CuK\alpha$ (1.5406 A°) radiation, the Bragg diffraction angle and the full width at half maximum (FWHM) of (112) diffraction peak. Results showed that for an annealing temperature of 350 °C, 450 °C and 550 °C, the worked out grain sizes are 62.185 nm, 53.565 nm and 74.958 nm, respectively. The composition of Cu-Zn-Sn precursors and CZTSe thin films obtained by EDS measurements are summarized in Table 1. As can be seen, after annealing at 550 °C for 30 minutes, the elements composition of $Cu/(Zn+Sn)$ is enhanced to 1.03 and the $Se/(Cu+Zn+Sn)$ ratio is very close to that of CZTSe compound.

Table 1. Chemical composition of the CZT precursor and CZTSe thin films.

Samples ID	Elemental composition (at.%)				Composition ratio	
	Cu	Zn	Sn	Se	Cu/(Zn + Sn)	Se/(Cu+Zn+Sn)
Cu–Zn–Sn precursor	49.44	23.74	26.82	-	0.97	-
CZTSe- 450 °C	22.39	11.72	12.28	53.61	0.93	1.15
CZTSe- 550 °C	24.16	10.91	12.56	52.37	1.03	1.09

On the other hand, a slight deficiency in Zn composition was observed in the precursors due to the strong suppression of Zn ions discharge during the electrodeposition process, and the amount of Zn is further reduced after annealing process. Similar results were reported by other research groups [28, 29]. However, it is established that the crystal structures of CZTSe (JCPDS# 01-070-8903) and secondary phases such as ZnSe (JCPDS# 65-7409), Cu_2SnSe_3 (JCPDS# 65-7524), and $Cu_{2-x}Se$ (JCPDS# 6-680) are nearly overlapped, so it is hard to make distinction between them [30]. Thus, to confirm the presence of CZTSe compound, the samples were analyzed further through Raman scattering measurements. Figure 3 shows the Raman spectra acquired from different points of the surface of an electrodeposited CZT+Se sample annealed under vacuum at 450 °C and 550 °C. Fortunately, the main Raman scattering signals of ZnSe near 250 cm^{-1} [31] and $Cu_{2-x}Se$ at 260 cm^{-1} [32] are not detected here, and CZTSe is almost the only phase presenting the most intense resonance peaks observed at around 171, 195 and 233 cm^{-1} [Fig. 3(a)].The result is in a good agreement with the Raman mode observed for CZTSe [10, 11, 33]. The Raman peak observed at 180 cm^{-1} at very small islands observed on the crystallites surface [Fig. 3(b)] is ascribed to traces of Cu_2SnSe_3 secondary phase [1, 34]. The presence of this phase in addition to $Cu_2ZnSnSe_4$ could be due to Zn deficiency as reported by Mangorian-friedlmeier *et al*. [35]. It was also found [36] that when the metallic elements

are present in the precursor in the ratio Cu:Zn:Sn = 2:1:1, the Cu_2SnSe_3 phase might form in parallel to $Cu_2ZnSnSe_4$.

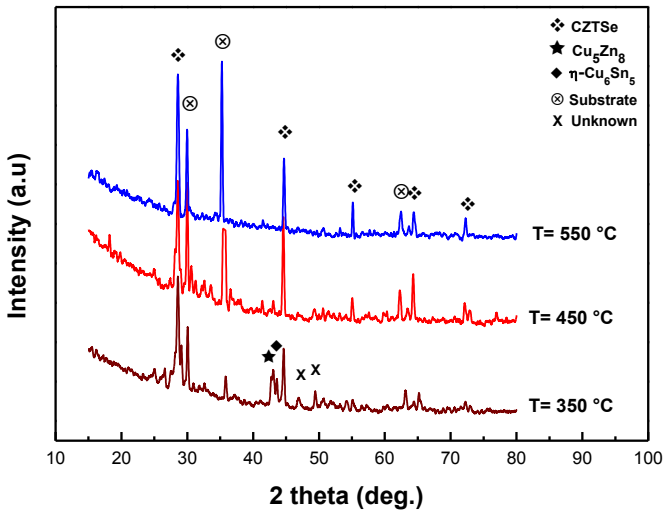

Figure 2. XRD patterns of CZTSe samples after annealing under vacuum for 30 min. Deposition potential: -1100mV.vs CSE

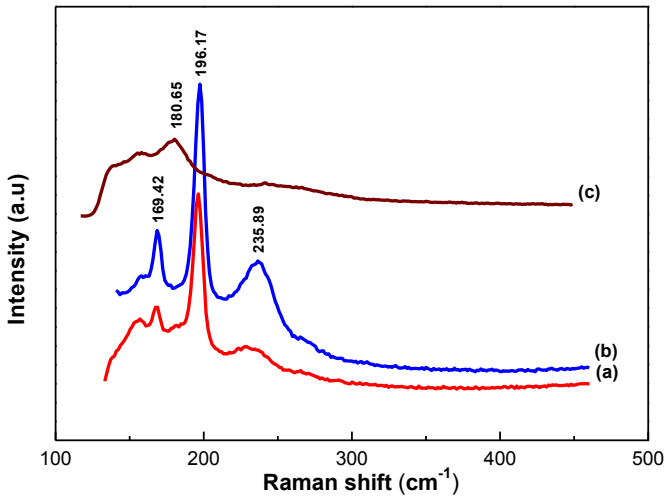

Figure 3. Room temperature Raman scattering spectra of CZTSe thin films after 30 min vacuum annealing at (a) 450 °C, (b) 550 °C and (c) Cu_2SnSe_3 phase detected on the surface of the deposits.

3.3. Surface morphology

The scanning electron micrographs reported in [Fig. 4(a)] display the morphology of the ternary CuZnSn precursors obtained at -1.1 V. vs.CSE. A mixture of clusters of small crystallites sized between 100 and 200 nm and 3D-dendritic micro crystals with various dimensions has been obtained. Image of selenium thin layer electrodeposited on the top of CZT alloy used as substrate is shown in [Fig. 4(b)]. From this, it is observed that the grains are almost uniform with an average grain size of

0.2 µm. The as-prepared CZT+Se precursors, after annealing under vacuum at 450 °C reveal a great crystallinity, have uniform, rough and dense morphology with a strong adhesion to ITO substrates [Fig. 4(c)]. The cross-sectional view of the same film annealed at 550 °C for half an hour [Fig.4(d)] indicate that films have a uniform and compact and denser morphology with closely packed grains. The presence of Cu_2SnSe_3 secondary phase on the surface of the deposit is clearly seen as small islands on the crystallites surface [see inset of [Fig.4(d)].The thickness of the prepared CZTSe layers was determined from the cross-sectional imaging was evaluated to ~1µm.

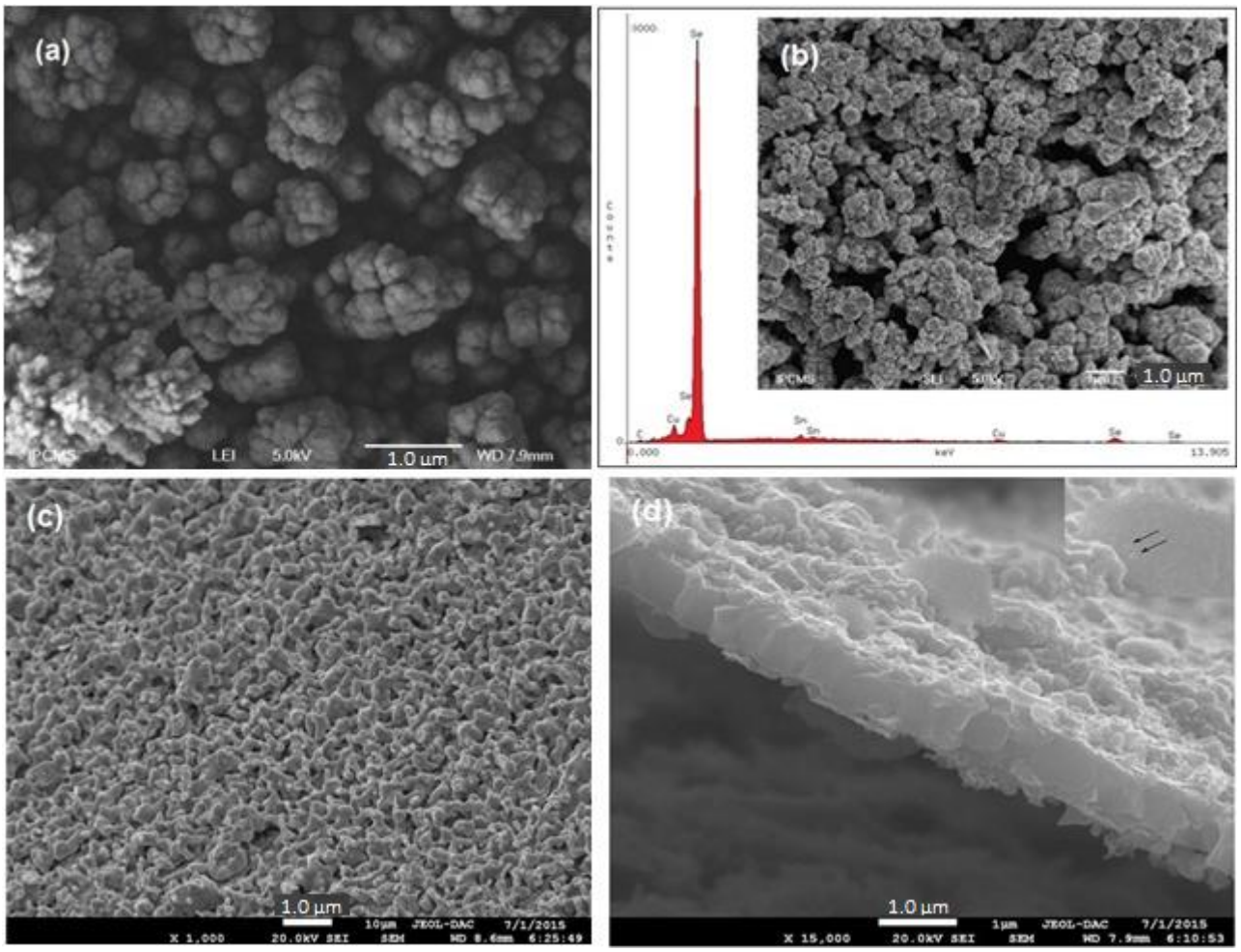

Figure 4. FESEM of (a) CZT thin films deposited at -1100 mV vs. CSE, (b) selenium thin layer electrodeposited on the top of CZT (-800 mV vs. CSE), (c) top view of CZTSe grains formed after annealing of CZT+Se under vacuum at 450C° and (d) cross-section of the same deposit annealed for 30 min at 550°C.

3.4. Optical properties

The absorption coefficient (α) is defined by the Lambert-Beer law and can be calculated from the absorbance data by means of the following equation [37]:

$$\alpha = 2.3.\frac{A}{t}$$

Where *A* is the absorbance and *t* is the film thickness.

Figure 5(a) presents the absorption coefficient of CZTSe thin films as a function of the annealing temperature. All films showed high absorption coefficients larger than 10^4 cm^{-1} at energies between 1.1 and 3.75 eV.

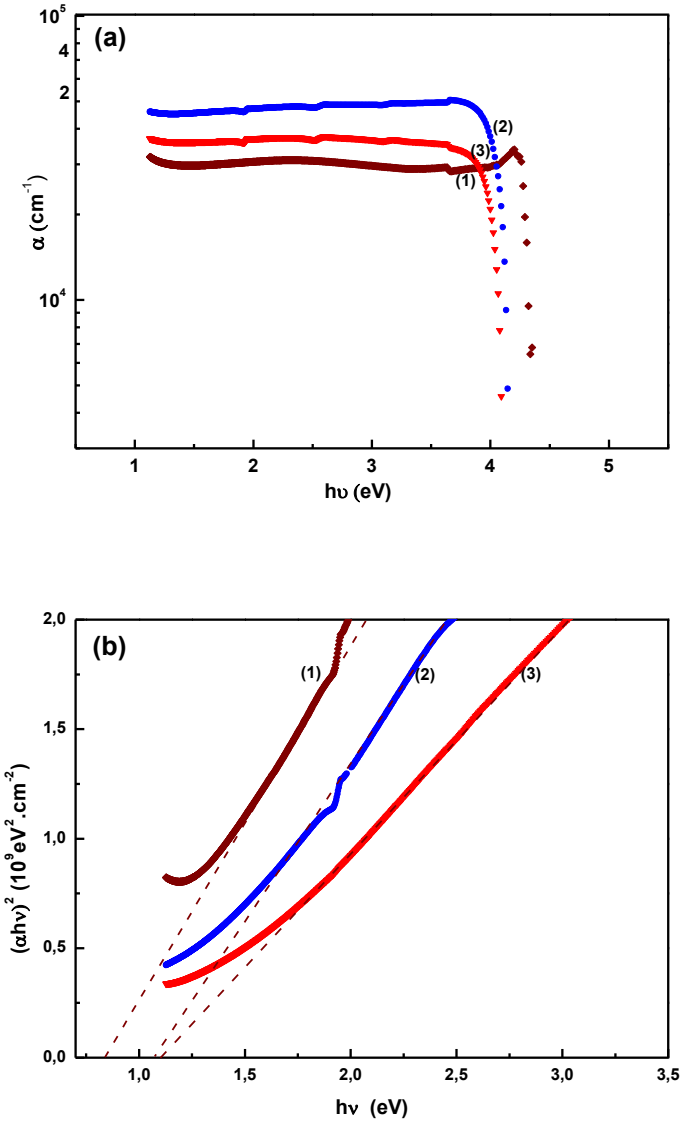

Figure 5. (a) Absorption coefficient spectra and (b) Tauc plots of CZTSe thin films annealed under vacuum at: (1) 350 °C, (2) 450 °C and (3) 550 °C.

As it is known, CZTSe has a direct ban gap which allows electronic transitions between the valence and conduction band to proceed without the intervention of phonons. Tauc and Davis-Mott plots [38, 39] were used to determine the optical gaps of the films. For that, the absorption coefficient in the strong absorption edge obeys [40]:

$$(\alpha h\upsilon) = A_0\,(h\upsilon - E_g)^{1/2}$$

Where *hν* is the photon energy, E_g is the optical bandgap of the material, and A is a parameter that depends upon the transition probability. Therefore, from the plot of $(\alpha h\nu)^2$ versus *hν*, the bandgap

can be determined by extrapolating the linear portion of the plot which denotes the onset of absorption, to the intercept with the energy-axes. The plots are given in Figure 5(b). From these graphs, it can be observed that the value of energy band gap of the films deposited at -1050 mV comes out to be 0.85, 1.04 and 1.06 eV for heat treatment under vacuum at 350 °C, 450 °C and 550 °C respectively. Similarly, for samples deposited at -1100mV.vs CSE), the obtained values of optical band gap are 0.84, 1.08 and 1.12 eV, respectively and are in good agreement with reported values for CZTSe [1,41,42]. The slight band gap deviation for the sample annealed at 350 °C can be attributed to Cu_2SnSe secondary phase which has a band gap around 0.84 eV [43].

When the annealing temperature is raised over 450°C, no significant changes were observed in bang gap values, indicating that that the most appropriate annealing conditions improving the crystalline structure of the films correspond to a temperature of around 450 °C. Moreover, these results agree well with the schemes reported by Ganchev *et al*. [11] and Fella *et al*. [33] on the evolution of phase formation during vacuum annealing. Hence, the formation of binary compounds (Cu_2Se, CuSe, SnSe and ZnSe) takes place for temperatures below 350 °C:

$$Cu + 2Se \rightarrow Cu_2Se \quad (1)$$

$$Sn + 2Se \rightarrow SnSe_2 \quad (2)$$

$$Zn + Se \rightarrow ZnSe \quad (3)$$

When the annealing temperature rises up to ~ 450 °C, the remaining metallic alloys react with selenium:

$$2\,Cu_5Zn_8 + 21Se \rightarrow 5Cu_2Se + 16\,ZnSe \quad (4)$$

$$Cu_6Sn_5 + 13Se \rightarrow 3Cu_2Se + 5\,SnSe_2 \quad (5)$$

The binaries react to form Cu_2SnSe_3 which in turn adsorbs ZnSe and forms the quaternary $Cu_2ZnSnSe_4$:

$$Cu_2Se + SnSe_2 \rightarrow Cu_2SnSe_3 \quad (6)$$

$$Cu_2SnSe_3 + ZnSe \rightarrow Cu_2ZnSnSe_4 \quad (7)$$

Obviously, in the case of Zn-poor deposit as revealed by EDS analysis, the reaction (7) does not pass up to the last and gives an idea of how to explain the phase composition revealed by XRD and Raman backscattering analysis.

4. CONCLUSION

A simple two-step method which combined electroplating and annealing under vacuum without use of hazardous selenium or H_2Se vapors was developed to prepare CZTSe thin films. Compared with the approaches based on co-evaporation and sputtering deposition, this method significantly simplifies the equipments and processes and reduces the cost. We successfully deposited CZTSe on ITO/glass substrates by sequential electrodeposition of CZT+Se followed by heat treatment under vacuum. Crack-free deposits with compact dense morphology were obtained. The structural investigation of annealed CZT+Se films at 350 °C resulted in the formation of CZTSe with the main peaks of (112), (204) and (312) in addition to secondary phases. The band gap, estimated using the Tauc and Davis-Mott model was as low as 0.84 eV suggesting the presence of Cu_2SnSe_3. With increasing the

temperature up to 550 °C, the measured band gap increased up to 1.12 eV and Raman spectra became typical of CZTSe compound. The secondary phases gradually disappeared, excepted small traces of Cu_2SnSe_3 whose presence was detected by Raman spectroscopy and FESEM analysis.

ACKNOWLEDGEMENTS
The authors wish to acknowledge the financial support of the Algerian Ministry of Higher Education and Scientific Research (Project CNEPRU- E01220110030). They would like to thank Prof. Boudissa (Mokhtar) for providing help in Raman spectroscopy investigations.

References

1. M. Grosberg, J. Krustok, K. Timmo, M. Altoosar, *Thin Solid Films,* 517 (2009) 2489
2. S. Siebentritt, S. Schorr, *Prog. Photovoltaics,* 20 (2012) 512.
3. I. Repins, C. Beall, N. Vora, C. DeHart, D. Kuciauskas, P. Dippo, B. To, J. Mann, W.C. Hsu, A. Goodrich, R. Noufi, *Sol. Energy Mater. Sol. Cells,* 101 (2012) 154.
4. B. Shin, O. Gunawan, Y.Zhu, N.A. Bojarczuk, S.J. Chey, S. Guha, *Prog. Photovolt.: Res. Appl.,* 21(1) (2013) 72.
5. G. S. Babu, Y. B. Kishor Kumar, P. U. Bashkar, V. S. Raja, *J. Phys. D: Appl. Phys*., 41 (2008) 205305 (7pp).
6. G. S. Babu, Y. B. Kishor Kumar; P. U. Bashkar; S. R. Vanjari, *Sol. Energy Mater. Sol. Cells,* 94 (2010) 221.
7. G. Brammertz, M. Buffière, Y. Mevel, Y. Ren, A.E. Zaghi, N. Lenaers, Y. Mols, C. Koeble, J. Vleugels, M.Meuris, J. Poortmans, *Appl. Phys. Lett*. 102 (2013) 013902.
8. L. Sun; J. He, H. Kong; F. Yue, P. Yang, J. Chu, *Sol. Energy Mater. Sol. Cells,* 95 (2011) 2907.
9. S. Kim, J. Kim, *Thin Solid Films,* 547 (2013) 178.
10. M. Ganchev, L. Kaupmees, J. Iliyna, J. Raudoja, O. Volobujeva, H. Dikov, M. Altosaar, E. Mellikov, T. Varema, *Energy Procedia*, 2 (2010) 65.
11. M. Ganchev, J. Iliyna, L. Kaupmees, T. Raadik, O. Volobujeva, A. Mere, M. Altosaar, J. Raudoja E. Mellikov, *Thin Solid Films,* 519 (2011) 7394.
12. M. Meng, L. Wan; P. Zou, S. Miao, J. Xu, *Applied Surface Science*, 273 (2013) 613.
13. R. Kondrotas, R. Juškėnas, A. Naujokaitis, G. Niaura, Z. Mockus, S. Kanapeckaitė, B. Čechavičius,K. Juškevičius, E. Saucedod, Y. Sánchez, *Thin Solid Films,* 589 (2015) 165.
14. W. Septina, S. Ikeda, A. Kyoraiseki, T. Harada, M. Matsumura, *Electrochim. Acta,* 88 (2013) 436.
15. J. Marquez-Prieto and I. Forbes, *Mater; Res. Innov.,* 18(7) (2014) 515.
16. Z. Chen, L. Han; ; L. Wan, C; Zhang, H. Niu, J. Xu, *Appl. Surf. Sci.,* 257 (2011) 8490.
17. S. Delbos, M. Benmoussa, R. Bodeux, C. Gougaud, N. Naghavi, *Thin Solid Films,* 589 (2015) 508.
18. M. Slupska, P. Ozga, *Electrochim. Acta,* 141 (2014) 149.
19. Southampton Electrochemistry Group in: T.J. Kemp (Ed.), *Instrumental Methods in Electrochemistry,* Ellis Horwood Ltd, Chichester, UK (1985).
20. 20. R. Modolo, M. Traore, O. Vittori, *Electrochim. Acta,* 31 (1986) 859.
21. Y. Lai, F. Liu, J. Li, Z. Zhang, Y. Liu, *J. Electroanal. Chemistry* 639 (2010) 187.
22. R. Kowalik, *Arch. Metal. Materials* 59 (2014) 871.
23. M.C. Santos, S.A.S. Machado, *J. Electroanal. Chem*. 567 (2004) 203.
24. D. Nam, A.S. Opanasyuk, P.V. Koval, A.G. Ponomarev, A. R. Jeong, G. Y. Kim, W. Jo, H. Cheong, *Thin Solid Films,* 562 (2014) 109.
25. B. R. Sankapal, S. D. Sartale, M. C. Lux-Steiner, A. Ennaoui, *Compt. Rend. Chim*., 9 (2006) 702.
26. S. Kundu, P. K. Biswas, , *Chem. Phys. Lett.*, 414 (2005) 107.
27. B.D. Cullity, S.R Stock, *Elements of X-ray diffraction,* 3rd ed., New Jersey: Prentice Hall (2001).

28. Z. Chen, L. Han, L. Wan, C. Zhang, H. Niu, J. Xu, *Appl. Surf. Sci.* 257 (2011) 8490.
29. P.M.P. Salomé, P.A. Fernandes, A.F. da.Cunha, *Phys. Status Solidi C*, 7 (2010) 913.
30. P.M. P. Salomé, P.A. Fernandes, A.F. da Cunha, *Thin Solid Films*, 517 (2009) 2531.
31. K. R. Murali, K. Thilakvathy, S. Vasantha, R. Oomen, *Chalcogenide Lett*., 5(6) (2008) 111.
32. E. Filippo, D. Manno, A. Serra, *J. Alloys Compd*., 538 (2012) 8.
33. C. M. Fella, A. R. Uhl, C. Hammond, I. Hermans, Y. E. Romanyuk, A. N. Tiwari, *J. Alloys Compd*., 567 (2013) 102.
34. T. C. Liu and Y. Hu, *Int. J. Electrochem. Sci*., 9 (2014) 2985.
35. T. M. Friedlmeier, N. Wieser, Th. Walter, H. Dittrich, H.W. Schock, *14th Europ. Photovolt. Sol. En. Conf.*, Barcelona (1997) 1242.
36. F. Hegert, R. Hock, *Thin Solid Films*, 515 (2007) 5953.
37. X. Li, H. Zhu, J. Wei, K. Wang, E. Xu, Z. Li, D. Wu, *Appl. Phys. A*, 97 (2009) 341.
38. J. Tauc, Optical Properties of Solids, Plenum, New York (1969).
39. N. F. Mott, E. A. Davis, Electronic Processes in Noncrystalline Materials, Clarendon, Oxford (1979).
40. S. Adachi, *Optical Properties of crystalline and amorphous semiconductors. Materials and Fundamental Principles*, Springer Science & Business Media, New York (1999).
41. S. Ahn, S. Jung, J. Gwak, A. Cho, K. Shin, K. Yoon, D. Park, H. Cheong, J.H. Yun, *Appl. Phys. Lett.*, 97 (2010) 021905.
42. D. Park, D. Nam, S. Jung, S. An, J. Gwak, K. Yoon, J.H. Yun and H. Cheong, *Thin Solid Films*, 519 (2011) 7386.
43. D. H. Kuo, W. D. Huang, Y. S. Huang, J. D. Wu, Y. J. Lin, *Surf. Coat. Tech.*, 205 (2010) S196.